Investigations of the Magnetocaloric and Thermal Expansion Properties of the Ln$_3$(adipate)$_{4.5}$(DMF)$_2$ (Ln = Gd−Er) Framework Series

Patrick W. Doheny, Simon J. Cassidy, and Paul J. Saines*

ACCESS | Metrics & More | Article Recommendations | SI Supporting Information

ABSTRACT: The development of sustainable and efficient cryogenic cooling materials is currently the subject of extensive research, with the aim of relieving the dependence of current low-temperature cooling methods on expensive and nonrenewable liquid helium. One potential method to achieve this is the use of materials demonstrating the magnetocaloric effect, where the cycling of an applied magnetic field leads to a net cooling effect due to changes in magnetic entropy upon application and removal of an external magnetic field. This study details the synthesis and characterization of a Ln$_3$(adipate)$_{4.5}$(DMF)$_2$ series (where Ln = Gd−Er) of metal−organic framework (MOF) materials incorporating a flexible adipate ligand and their associated magnetocaloric and thermal expansion properties. The magnetocaloric performance of the Gd$_3$(adipate)$_{4.5}$(DMF)$_2$ material was found to exhibit the highest magnetic entropy changes of the series, with a peak entropy change of 36.4 J kg^{-1} K^{-1} for a 5-0 T field change at a temperature of 2 K, which is suited for ultra-low-temperature cooling applications. Thermal expansion properties were also investigated within these materials, demonstrating modest negative and large positive thermal expansion identified along the different crystallographic axes within the MOF structures over a 100−300 K temperature range that demonstrated the novel mechanical properties of these adipate framework structures.
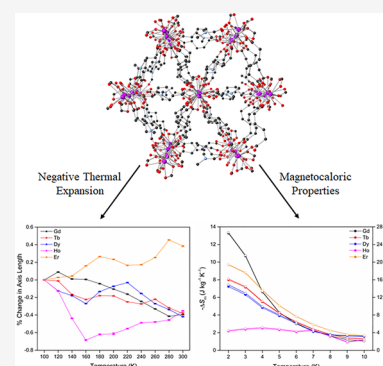
INTRODUCTION

Quantum computing, hydrogen liquefaction, and medical imaging applications are just a few of many diverse fields that require cooling to temperatures well below 80 K (the boiling point of liquid nitrogen).[1,2] To achieve this, liquid helium is routinely used to cool to temperatures down to 2 K, while dilution refrigerators, utilizing a mixture of ^{3}He and ^{4}He isotopes, can achieve even lower temperatures of 20 mK. Underlying this is the dependency on the use of liquid helium, an expensive and increasingly scarce resource that is (for all intents and purposes) nonrenewable, a significant monetary expense, and vulnerable to supply disruptions because of the major sources for this being currently limited to two countries.[3] The development of new materials capable of low-temperature cooling in lieu of liquid helium is thus an active area of research with the goal of relieving the dependence on the finite supply of helium and the development of cost-effective low-temperature cooling methods.

Magnetocaloric cooling is one means by which low-temperature refrigeration may be achieved, in which subjecting paramagnetic materials to a cycled magnetic field leads to an entropically driven solid-state cooling process.[4] First discovered in 1917,[5] materials exhibiting the magnetocaloric effect (MCE) have since been extensively studied in the context of both fundamental scientific interest[6,7] and practical applications.[8] As the MCE is dependent on a magnetic entropy

change upon cycling of an applied magnetic field, lanthanide-based materials are ideal magnetocaloric candidates due to their large number of unpaired spins, which leads to higher magnetic entropy changes. While materials such as oxides[9−11] and metal clusters[12−14] have demonstrated impressive magnetocaloric properties, including the benchmark Gd$_3$Ga$_5$O$_{12}$ (GGG) material, coordination polymers including metal−organic frameworks (MOFs) offer the ability to tailor magnetic properties by virtue of directed topological design targeting high magnetic density, rapid magnetization at low fields, and suppression of long-range magnetic ordering, which is not easily achievable in other classes of materials.[15,16] Examples of such materials include Gd(HCOO)$_3$, Gd(OH)-CO$_3$, and GdPO$_4$, which demonstrate magnetic entropy changes greater than those found in the benchmark GGG material due to the high density of magnetic ions within their structures.[17−19]

This report details the synthesis and characterization of a series of Ln$_3$(adipate)$_{4.5}$(DMF)$_2$ (Ln = Gd−Er) frameworks, of
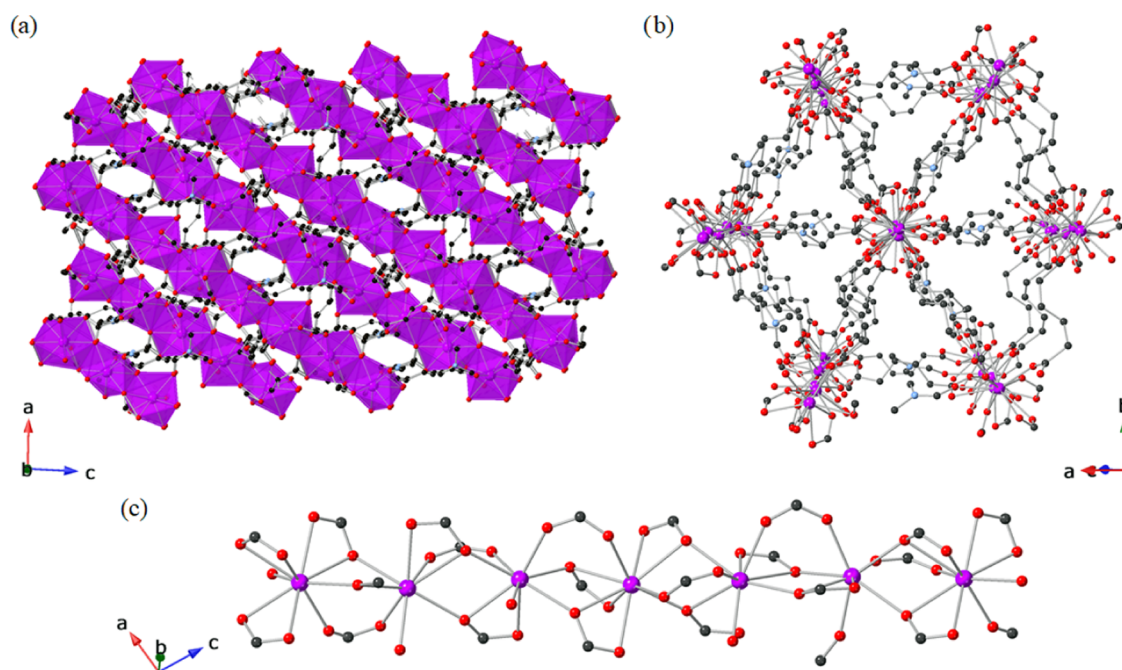
Figure 1. Crystal structure of $Gd_3(adipate)_{4.5}(DMF)_2$ showing (a) the *ac* plane in which large positive and negative thermal expansion occurs, (b) the distorted triangular pores, and (c) the extended Gd chain. The disorder components and hydrogen atoms have been omitted for clarity. Atom labeling: Gd = purple, O = red, N = blue, and C = gray.

which the synthesis and crystal structure of the Tb analogue has been reported previously,[20] that incorporate a flexible adipate ligand leading to thermal expansion properties that demonstrate uniaxial negative thermal expansion. This isostructural series exhibits a layered structure of Ln chains, linked by adipate ligands, that remain paramagnetic to 1.8 K in the absence of an applied magnetic field, although there is evidence for field-induced weak ferromagnetic ordering of the Dy phase. Magnetization measurements revealed a wide range in MCE performance with the magnetic entropy change maximized for the Gd-based material at 2 K that is attributed to the high spin number and lack of spin−orbit coupling that is characteristic of the Gd(III) ion.

RESULTS AND DISCUSSION

Synthesis and Structure. The $Ln_3(adipate)_{4.5}(DMF)_2$ series was synthesized following a previously published procedure for the terbium analogue.[20] The $Ln(NO_3)_3 \cdot xH_2O$ salt and adipic acid were dissolved in DMF and were heated at 153 °C for 24 h in a Teflon-lined autoclave. After cooling to room temperature blocklike crystals of between ~1×10^{-4} and ~1×10^{-3} mm^3 were obtained that were suitable for single-crystal X-ray diffraction studies of the Gd−Er series. The Gd, Dy, Ho, and Er materials were found to be isostructural to the previously reported Tb analogue (see Tables S1−S5 for crystallographic details) with all five structures crystallizing in the $P2_1/n$ space group with asymmetric units (Figures S1−S5) composed of three Ln atoms, 4.5 adipate ligands, and two DMF molecules. The structures were characterized by Ln(III) ions that were coordinated by the carboxylate groups of the adipate ligands to form Ln(III) chains of edge-sharing polyhedra with neighboring chains bridged by adipate ligands to form a connected 3D network of Ln chains that define the corners of distorted triangular channels (Figure 1).

The coordination sphere of two of the three Ln(III) ions in the asymmetric unit were capped by a single DMF molecule to

yield a formula of $Ln_3(adipate)_{4.5}(DMF)_2$ with thermogravimetric analysis (TGA), confirming this stoichiometry (Figures S6−S10) and bond valence sum analysis[21] (Table S6) of each structure consistent with trivalent Ln nodes. The Ln(III)−Ln(III) distance ions within the chains was found to reach a maximum of 4.0382(3), 4.0587(3), and 4.0043(3) Å (for the Gd1−Gd2, Gd2−Gd3, and Gd3−Gd1 distances respectively) and gradually decrease across the series to a minimum of 3.8576(3), 3.9701(3), and 4.0043(3) Å (Er1−Er2, Er2−Er3, and Er3−Er1). The magnetic coupling in these materials is expected to be governed by their superexchange distances, i.e., the shortest magnetic coupling distance via the oxygen atoms linking Ln cations, (Table S7) and their associated angles (Table S8), in the Ln chains were comparable across the series with the distances ranging from 4.731(7) to 4.992(4) Å and angles from 104.65(8) to 111.64(14)°. The members of the framework series exhibited modest densities with a minimum of 1.963 g/mL found for $Gd_3(adipate)_{4.5}(DMF)_2$ and a maximum of 2.045 g/mL for $Er_3(adipate)_{4.5}(DMF)_2$ at 300 K.

Bulk samples of each framework for analysis were obtained by grinding the single crystals of each into a bulk powder with phase purity assessed by Le Bail fitting of the resulting X-ray powder diffraction patterns to the single-crystal X-ray structures (Figures S11−S15) supported by elemental analysis results (see the Supporting Information). Analysis of the powder diffraction patterns revealed that although the Gd- and Tb-based materials were phase pure, the powder diffraction patterns of the Dy, Ho, and Er phases showed a peak at a low angle (~5.52° 2θ). As we were unable to find a phase that matched this impurity peak from patterns in the International Centre for Diffraction PDF-2[22] and it did not match patterns calculated from the known structures of simple organic phases, this is thought to be possibly due to the presence of an unidentified metal−organic compound, which is likely to be paramagnetic rather than diamagnetic in nature. It should be noted that there is a small difference between the lattice

parameters determined at ambient temperature using single-crystal diffraction and powder diffraction studies, with the parameters determined for powder diffraction studies typically the smaller of the two. We note that it is not unusual for there to be some variation in the absolute values of lattice parameters determined using different instruments. In the absence of the use of a calibration reference material by, e.g., addition to a powder sample, it is the relative change in lattice parameters with external stimuli rather than their absolute values that provide the primary insight into a material.

Thermal Expansion Properties. The presence of the flexible adipate ligand within the framework structures made the $Ln_3(adipate)_{4.5}(DMF)_2$ series promising candidates for the novel thermal expansion properties. To explore this possibility, variable temperature single-crystal X-ray diffraction was used to explore the structural changes over a temperature range of 100−300 K with cell parameters acquired at 10 K intervals. The temperature-dependent changes in cell parameters were analyzed using the PASCal program,[23] with the calculated coefficients of thermal expansion along the principal crystallographic axes summarized in Table 1 with the lattice parameters from which these are extracted given in Tables S9−S13.
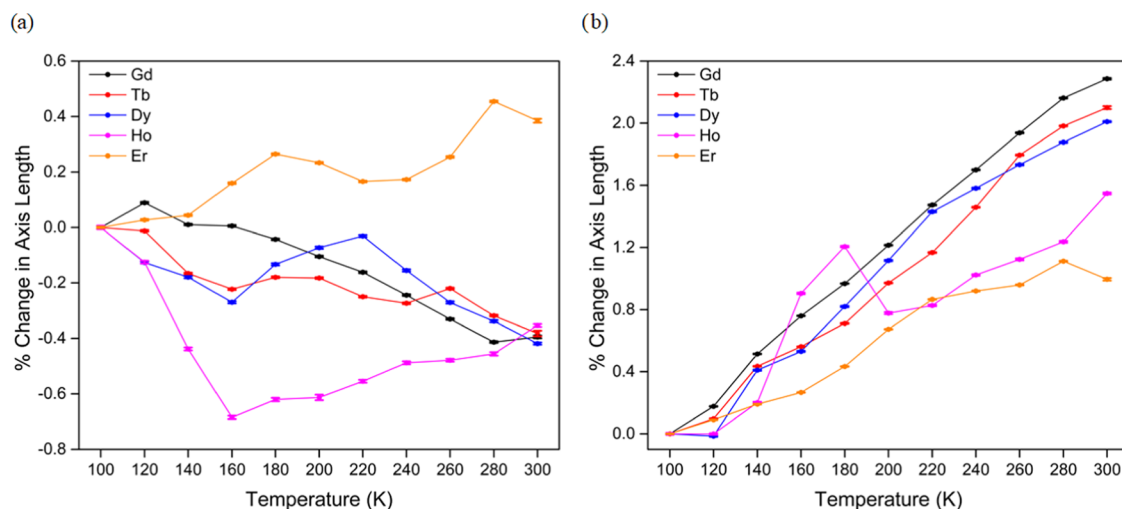
Table 1. Coefficients of Thermal Expansion Along the Principal Axes of the $Ln_3(adipate)_{4.5}(DMF)_2$ Series

| Ln	X_1 (∼c-axis), MK^{-1}	X_2 (b-axis), MK^{-1}	X_3 (a-axis), MK^{-1}
Gd	−23(3)	48(2)	120(3)
Tb	−16(2)	43(3)	110(3)
Dy	−11(4)	51(5)	113(5)
Ho	−18(12)	36(9)	80(9)
Er	65(6)	62(5)	19(2)

With the exception of the Er material, the thermal expansion properties of adipate frameworks demonstrated anisotropic negative thermal expansion (NTE) along the principal axis X_1 (Figure 2a) and positive thermal expansion (PTE) along the X_2 and X_3 axes (Figures 2b and S16). The principal axes of X_2 and X_3 coincide with the unit cell b- and a-axes, while the third, X_1, is slightly offset from the c-axis (see Tables S14−S18 for projection vectors); for clarity to the reader, trends across the

series from here will refer to these principal axes by the crystallographic axis they are closest to. The relative magnitude of the NTE was found to reach a maximum in the Gd material with an NTE coefficient of $\alpha_c = -23(3)$ MK^{-1} and then generally decrease with decreasing ionic radii of the lanthanides;[24] we note that the larger error associated with the values determined for the Ho phase makes comparing the size of this to other members of the series difficult. We believe that this arises from lower accuracy in the lattice parameters determined from the single-crystal studies of the Ho phase, likely due to crystal movement during data collection, rather than meaningful fluctuations. Unexpectedly, with the exception of the Er phase, the a-axis of these materials demonstrated large PTE with a maximum α_a of 120(3) MK^{-1} found for the Gd compound. In contrast to the first four members of the series, the Er material displayed purely PTE behavior with thermal expansion coefficients of 65(6), 62(5), and 19(2) MK^{-1} for principal axes along approximately the c-, b- and a-axes, respectively.

The thermal expansion of these frameworks can be rationalized as arising from a combination of the expansion of its struts (in this case, the edge-sharing Ln chains tightly bound by adipate linkers) with temperature and the hinging of the framework angles with respect to temperature; a structural mechanism that has been previously used to rationalize analogous thermal expansion behavior in other framework materials.[25−28] Using the Gd material (which demonstrates the largest NTE and PTE within the ac plane) as an example, these hinging angles (see Figure S17) are defined by neighboring Gd1 cations within a chain and Gd1 of the neighboring chain to which these are connected by the adipate linker (these adipate linkers provide the only interchain connectivity within the ac plane). These two key angles θ_c and θ_a connect Gd cations along the principal axis directions for which thermal expansion occurs. A hinging angle increase will drive increased positive thermal expansion in that direction, while a hinging angle decrease leads to smaller positive or negative thermal expansion along that direction. The θ_c angle that connects Gd cations along the c direction decreases from 119.3316(14)° at 100 K to 118.001(4)° at 300 K, while the θ_a angle along the a-axis increases from 60.5378(14)° at 100 K to 61.871(9)° at

Figure 2. (a) Relative change in c- and (b) relative change in a-axis lengths of the $Ln_3(adipate)_{4.5}(DMF)_2$ materials. The error bars are smaller than the data points.
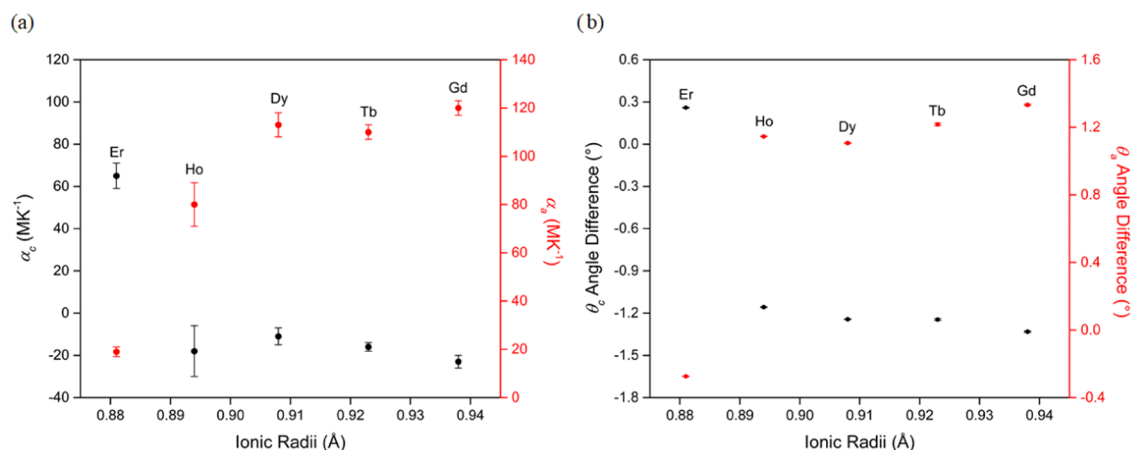
Figure 3. (a) Coefficients of thermal expansion of the c- and a-axis and (b) the θ_c and θ_a hinging angle differences for the $Ln_3(adipate)_{4.5}(DMF)_2$ series as a function of Ln(III) ionic radii. The error bars in (b) are smaller than the data points.

300 K (Figure S18). The decrease in θ_c principally leads to NTE, while the increase in the θ_a angle primarily leads to PTE, which is greater than that caused by expansion of the framework struts (inorganic chains and adipate linkers) alone. In contrast, there is only a smaller change in these framework angles (Figure S19) in the $Er_3(adipate)_{4.5}(DMF)_2$ material from 63.5406(14) and 116.272(15)° at 100 K to 63.2662(18) and 116.5317(19)° at 300 K. This leads to the isotropic thermal expansion properties of the Er material where framework hinging is negligible and its PTE along all three principal axes arises from the expansion of the Er chains and adipate linker struts. A comparison of the c-axis coefficients of thermal expansion with the ionic radii of the Ln(III) ions reveals a clear dependence of the NTE on cation size (Figure 3a) with larger ionic radii correlated with larger NTE. The difference in the θ_c hinging angles at 100 and 300 K (Figure 3b) are also similarly correlated with ionic radii in that the largest difference (and subsequently largest NTE) is found for the Gd material with the absolute difference subsequently decreasing to a minimum for the Er material.

In light of this, we suggest a potential mechanism for the decrease in NTE magnitude (within error) with decreasing Ln(III) size, which stems from a decrease in the tendency of the framework hinging angles, θ_c and θ_a, to change with temperatures across the series from Gd to Er. The smaller size of the Er(III) ion likely restricts the flexibility of its coordination polyhedra relative to the larger lanthanide cations, such as Gd(III), due to the shorter bonds between the Er(III) node and carboxylates of the adipate ligand, which in turn reduce the flexibility of framework hinging when compared to the bigger and less tightly bound Gd(III) nodes. This change in thermal expansion across the series with lanthanide ionic radii may enable other mechanical properties to be realized including zero thermal expansion of the c-axis by, for example, a doped $Ho_{1-x}Er_x(adipate)_{4.5}(DMF)_2$ series.

Magnetic Property Analysis. Field-cooled (FC) and zero field-cooled (ZFC) magnetic susceptibility data of the $Ln_3(adipate)_{4.5}(DMF)_2$ series was obtained in a 1000 Oe field over a 1.8−300 K temperature range. The FC and ZFC data for all five materials (Figures S20−S24) did not show any evidence of long-range magnetic order down to 1.8 K and were found to obey the Curie−Weiss law across the entire temperature range. Fitting of the Curie−Weiss law (Figures S25−S29) to the data, from 2 to 300 K, revealed Weiss

temperatures (Table 2) that imply weak ferromagnetic interactions for the Gd- and Er-based materials, while weak

Table 2. Weiss Temperatures, Effective and Theoretical Magnetic Moments of the $Ln_3(adipate)_{4.5}(DMF)_2$ Series

Ln	Weiss Temperature (K)	Effective μ_{eff} (μ_B)	Theoretical μ_{eff} (μ_B)
Gd	0.47(4)	7.7420(10)	7.94
Tb	−0.35(7)	9.628(3)	9.72
Dy	−1.50(6)	10.137(3)	10.65
Ho	−0.74(8)	10.340(3)	10.6
Er	0.86(6)	9.069(2)	9.58

antiferromagnetic interactions were suggested for the Tb-, Dy- and Ho-based materials; it must be noted that there may be contributions to this from low-temperature crystal field effects for the Tb−Er phases. The effective magnetic moments (μ_{eff}) of each material were all found to be consistent with the values predicted for trivalent lanthanide ions by the Russell−Saunders coupling scheme.[29] The low-temperature evolution of $\chi_M T$ is consistent with ferromagnetic coupling in the Gd and Er members of the series, with a significant increase observed below 10 K, while $\chi_M T$ for Ho decreases significantly, consistent with antiferromagnetic coupling (see insets of Figures S20, S23, and S24). Consistent with the Tb analogue having the lowest absolute value for its Weiss temperature, it has the smallest change in $\chi_M T$ with temperature, while that of the Dy phase decreases significantly below 20 K before increasing again below 3 K (see insets of Figures S21 and S22).

Isothermal magnetization measurements at 2 K (Figure 4) showed that these materials, with the exception of Ho, reached saturation magnetization (M_{sat}) at fields of 50 kOe with Gd demonstrating the highest M_{sat} value of the series (Figures S30−S34). At fields <10 kOe, the Er material was observed to magnetize faster than the other materials, while the Ho framework was found not to reach saturation even at the maximum applied field, likely a result of it having relatively strong antiferromagnetic interactions. It is expected that the M_{sat} values of powder samples of compounds with Heisenberg and Ising spins will be close to $g_J J$ and $g_J J/2$ respectively,[6,11,30] because, while the magnetic moment of a Heisenberg spin can be fully aligned with the applied magnetic field regardless of crystallite orientation, the restriction for Ising spins to point along the easy axis makes the extent of magnetization of an
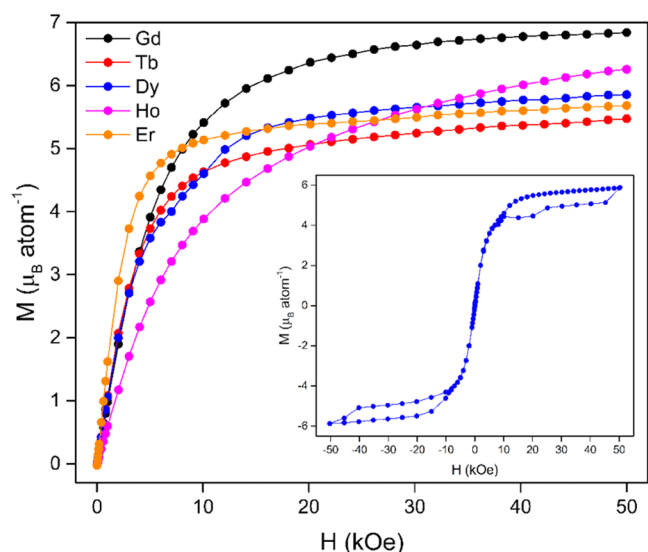
Figure 4. Isothermal magnetization curves of the $Ln_3(adipate)_{4.5}(DMF)_2$ series at 2 K. Inset: full magnetization loop of $Dy_3(adipate)_{4.5}(DMF)_2$ showing its magnetic hysteresis at 2 K.

individual crystallite dependant on its orientation compared to the applied magnetic field. Comparisons of the M_{sat} values with these predicted magnetization values suggest that the Gd material acts as a Heisenberg spin system. In contrast, the other four materials are more consistent with Ising systems, although their M_{sat} values are higher than that expected for a purely Ising system, suggesting some deviation from pure Ising behavior. The Dy material also displayed unexpected behavior with the full magnetization loop (Figure 4 inset) exhibiting metamagnetic hysteresis at 2 K, which was not observed at higher temperatures or in other compounds. FC measurements from 1.8 to 30 K were carried out at applied fields ranging from 1 to 30 kOe (Figure S35) to elucidate the origin of this behavior but were inconclusive. While this hysteresis may be ascribed to the presence of the paramagnetic impurity phase, we note that the magnetic properties observed across the other members of this series, including the Gd and Tb phases, which appear phase pure, and the Ho and Er materials, which contains this impurity phase, suggests that this is less likely. Thus, we propose that the hysteresis arises from the intrinsic behavior of the Dy phase varying its behavior compared to other members of the series, either due to differences in its superexchange pathways or its electron count modifying its magnetic interactions, single-ion anisotropy, or crystal field effects. This is in contrast with all other materials examined during this study whose magnetization curves are consistent with paramagnetic behavior at 2 K and all fields examined during this study. A tentative explanation assigns the hysteresis
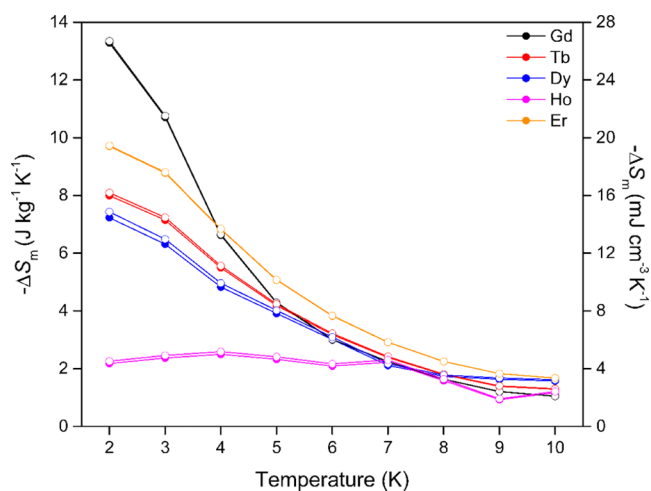
to a field-induced magnetic phase transition to a ferrimagnetic or canted antiferromagnetic phase. Either case would be consistent with the small rise in $\chi_M T$ observed at very low temperatures, suggesting that it may be on the cusp of this transition at more modest fields at 1.8 K. Clear confirmation of the precise nature of this state requires analysis of the magnetic structure of the Dy phase under applied magnetic fields, which was not pursued further during the current study due to the high hydrogen content of these materials and the difficulties anticipated in deuteration. Another method by which more insight into the origin of this metamagnetic behavior might be elucidated would be the use of magnetic relaxation measurements utilized in the study of single-molecule magnetism (SMM); this may highlight any single chainlike behavior which would also be consistent with the observed properties, but this was beyond the scope of this initial study which focuses on the magnetocaloric properties of these materials.

The magnetocaloric properties of the $Ln_3(adipate)_{4.5}(DMF)_2$ series were evaluated by their magnetic entropy changes (ΔS_m) between 2 and 10 K and magnetic field changes between 0 and 1−5 T, which were determined using the Maxwell relation $\Delta S_m(T) = \int [\partial M(T,B)/\partial T]_B dB$. Despite being an indirect method of evaluating magnetocaloric properties, it has been previously demonstrated that good agreement can be obtained between measurements using this and more direct means of gauging magnetocaloric performance via heat capacity measurements.[17,18] The maximum entropy change, $-\Delta S_m^{max}$, of $Gd_3(adipate)_{4.5}(DMF)_2$ phase is 36.4 J kg^{-1} K^{-1} at 2 K, a value comparable to the benchmark GGG material, which has a $-\Delta S_m^{max}$ of ~35 J kg^{-1} K^{-1} for a 5-0 T field change,[31] but relatively modest compared to other coordination polymers.[32,33] The low density of the $Gd_3(adipate)_{4.5}(DMF)_2$ structure leads to a much more modest $-\Delta S_m^{max}$ as a function of volume with the $-\Delta S_m^{max}$ of the other compounds being unremarkable for a field change of 5-0 T (Table 3).

The performance of magnetocalorics for small field changes is important as applied fields of 1−2 T can be generated using a permanent magnet, which avoids the need to use a superconducting magnet to achieve magnetic cooling. For a $\Delta B = 1$-0 T, the materials exhibited a maximum entropy change (Figure 5) at 2 K, with $Gd_3(adipate)_{4.5}(DMF)_2$ the highest with a $-\Delta S_m^{max}$ of 13.3 and 23.9 J kg^{-1} K^{-1} for $\Delta B = 2$-0 T (Figure S36). At higher temperatures, the entropy changes were observed to decrease quickly, which is consistent with the loss of magnetization at increasing temperatures. Notably, despite the Er material having a lower $-\Delta S_m^{max}$ of 9.7 J kg^{-1} K^{-1} at 2 K, the decrease in entropy change is much more gradual compared to the Gd phase with its performance remaining appreciably higher between 4 and 10 K, a commonly used temperature range for cryogenic cooling using liquid helium.

Table 3. Maximum Entropy Changes ($-\Delta S_m^{max}$) and Peak Temperatures (T_{max}) of the $Ln_3(Adipate)_{4.5}(DMF)_2$ Series at Different Field Changes

Ln	T_{max} (K)	$\Delta B = 1$-0 T		T_{max} (K)	$\Delta B = 5$-0 T	
		(J kg^{-1} K^{-1})	(mJ cm^{-3} K^{-1})		(J kg^{-1} K^{-1})	(mJ cm^{-3} K^{-1})
Gd	2	13.3	26.7	2	36.4	73.1
Tb	2	8.0	16.2	4	12.3	24.6
Dy	2	7.2	14.9	5	12.0	24.7
Ho	4	2.5	5.17	10	9.2	19.0
Er	2	9.7	19.5	4	12.5	25.2

Figure 5. Magnetic entropy changes of the $Ln_3(adipate)_{4.5}(DMF)_2$ series for ΔB = 1-0 T. The filled and open symbols denote mass and volumetric entropy units, respectively.

In contrast to the behavior observed for smaller field changes, the $-\Delta S_m^{max}$ for $Gd_3(adipate)_{4.5}(DMF)_2$ remains well above that of all other members of the series for field changes of 5-0 T up to 10 K (Figure 6). This is linked to the Gd
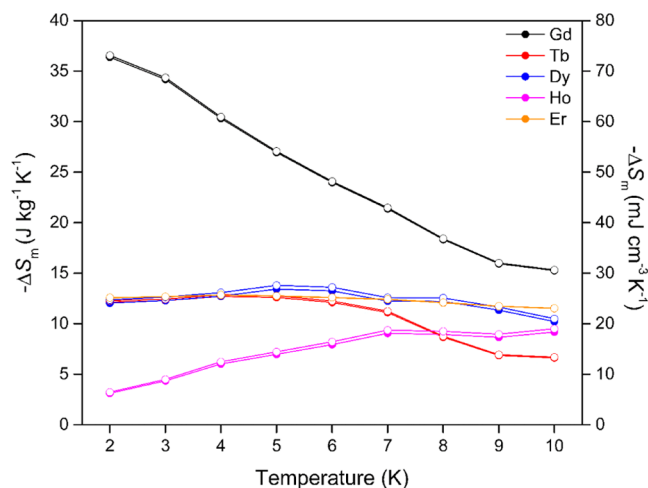
Figure 6. Magnetic entropy changes of the $Ln_3(adipate)_{4.5}(DMF)_2$ series for ΔB = 5-0 T, where the filled and open symbols denote mass and volumetric entropy units, respectively.

analogue having the highest magnetization under strong applied fields, while the other lanthanides have more rapid increases of magnetization under low applied fields, most notably Er whose magnetization approaches saturation at around 1 T. The greater ease of magnetization of $Er_3(adipate)_{4.5}(DMF)_2$ likely stems from the dominant magnetic coupling in this phase being ferromagnetic, as indicated by it having the highest Weiss constant among the series. The structure of the $Ln_3(adipate)_{4.5}(DMF)_2$ series suggests that the dominant magnetic coupling is likely to occur within the edge-sharing chains, which are likely ferromagnetic for $Er_3(adipate)_{4.5}(DMF)_2$. It has been shown that the MCE of frameworks can be optimized for lower fields and higher temperatures through the inclusion of ferromagnetic chains, although if this is the case here for $Er_3(adipate)_{4.5}(DMF)_2$, as indicated above, it would be the first time that ferromagnetic

chains in an Er material lead to an optimization of its MCE in this way.[6,30,34−38] Although the overall performance is modest, this suggests that Er-containing phases should not be neglected in the search for magnetocalorics optimized for use under low applied fields. Although beyond the scope of this study, the presence of anisotropic thermal expansion within this framework series may suggest another method of tuning the magnetic properties at low temperature, even if the change in unit cell dimensions with the temperature at which these materials are useful magnetocalorics might be quite small. For example, the application of pressure to the framework may be one means by which the magnetization and by extension, the magnetic entropy changes may be improved upon by changing the strength of the magnetic interactions in these materials.

Despite the relatively modest magnetocaloric properties being demonstrated by the members of this adipate framework series compared to other coordination polymers,[17−19] the results have demonstrated that well-isolated infinite Ln chains can be a viable platform for the development of magnetocaloric frameworks. Additionally, the unexpectedly high entropy changes of the Er material at low fields, coupled with its much slower decrease with increasing temperature, demonstrate the capability of Er(III) materials to act as viable magnetocalorics in lieu of more traditional Gd(III) systems. This is even in the absence of the frustrated interactions found in other Ising systems with similar enhanced performance for lower applied magnetic fields.[6,34,39]

◼ CONCLUSIONS

The magnetic and mechanical properties of a series of five $Ln_3(adipate)_{4.5}(DMF)_2$ frameworks have been characterized with a particular focus on their magnetocaloric performance over a 2−10 K temperature range and thermal expansion. The magnetic entropy changes of this isostructural series were examined over an applied magnetic field range of 5-0 T that identified the $Gd_3(adipate)_{4.5}(DMF)_2$ material as the best-performing member of the series. Magnetization measurements of the Gd material at 2 K revealed a maximum $-\Delta S_m^{max}$ of 36.4 J kg^{-1} K^{-1} for a field change of 5-0 T, which is significantly larger than other members of the series although the greater ease of magnetization of $Er_3(adipate)_{4.5}(DMF)_2$ leads to it having higher performance above 4 K for a more modest 1-0 T field change.

The thermal expansion properties of the five framework materials were also investigated using variable temperature single-crystal X-ray diffraction over a 100−300 K temperature range in which the members of the series (with the exception of the Er material) demonstrated anisotropic negative thermal expansion properties. The coefficients of thermal expansion demonstrated anomalous thermal expansion within the *ac* plane with significant NTE along a direction close to the *c*-axis, while the *a*-axis has very large PTE. Generally, the thermal expansion becomes more isotropic with decreasing ionic radii of the lanthanides as the framework hinging responsible for the NTE and large PTE decreases.

While the magnetocaloric properties of this framework series were modest compared with other Ln framework materials, this study has explored important design considerations for magnetocaloric framework materials. The use of flexible adipate ligands has led to a series of frameworks that demonstrate both magnetocaloric properties and novel thermal expansion behavior. The coexistence of these properties is one means by which the magnetocaloric attributes could be

enhanced, for example, the existence of anisotropic thermal expansion may indicate that the application of a stimulus such as pressure will also trigger anisotropic changes in the magnetic interactions that change their magnetocaloric behavior.

EXPERIMENTAL SECTION

General. $Gd(NO_3)_3 \cdot 6H_2O$ (Acros Organics, 99.9%), $Tb(NO_3)_3 \cdot 6H_2O$, $Dy(NO_3)_3 \cdot 5H_2O$, $Ho(NO_3)_3 \cdot 5H_2O$, $Er(NO_3)_3 \cdot 5H_2O$ (Alfa Aesar, 99.9%), adipic acid (Acros Organics, 99%), and N,N-dimethylformamide (Fisher Scientific, 99%) were obtained from commercial sources and used without purification unless otherwise stated. Elemental microanalysis was carried out at the CHN Microanalysis Service at University College London.

Framework Synthesis. All members of the $Ln_3(adipate)_{4.5}(DMF)_2$ framework series were synthesized according to a previously published procedure for the $Tb_3(adipate)_{4.5}(DMF)_2$ material with modifications.[20]

$Ln_3(adipate)_{4.5}(DMF)_2$. $Ln(NO_3)_3 \cdot 6H_2O$ (1.65 mmol) and adipic acid (232 mg, 1.59 mmol) were dissolved in DMF (5 mL), and the solution was sealed in a 25 mL Teflon-lined autoclave and heated at 153 °C for 24 h. After cooling to room temperature, the mixture was filtered and the solid was washed with DMF to yield the framework as a crystalline product (see the Supporting Information for yields and elemental analysis).

Physical Characterization and Instrumentation. *Single-Crystal X-ray Diffraction.* Single-crystal X-ray diffraction was performed using a Rigaku Oxford Supernova diffractometer equipped with an Oxford Cryosystems cryostream, an Atlas S2 CCD detector, and employing Mo Kα radiation generated using a sealed X-ray tube. All data was integrated within the CrysAlisPro software suite[40] with a face indexed absorption correction applied to the data of each collection. The structures were solved using SHELXT[41] with structural refinements carried out using SHELXL-2018/3[42] within the Olex2 graphical user interface.[43] All nonhydrogen atoms were refined anisotropically with the hydrogen atoms placed at calculated positions using a riding model. Crystallographic data are given in Tables S1–S4, and the CIFs have been deposited with the CCDC under deposition numbers CCDC 2124536–2124540.

Magnetometry. DC magnetic susceptibility and magnetization measurements were carried out using a Quantum Design MPMS SQUID magnetometer with samples sealed inside a gelatin capsule and mounted inside a plastic straw with a uniform diamagnetic background. Field-cooled and zero field-cooled magnetic susceptibility measurements were performed over a 1.8–300 K temperature range under an applied magnetic field of 1000 Oe, while isothermal magnetization data was acquired over a 2–10 K temperature range under applied fields ranging from −5 to 5 T.

ASSOCIATED CONTENT

ⓈⒾ Supporting Information

The Supporting Information is available free of charge at https://pubs.acs.org/doi/10.1021/acs.inorgchem.1c03688.

> Experimental details, crystallographic tables, DSC and TGA data, Le Bail fits of powder diffraction data, PASCal principal axis projection vectors, thermal expansion data, and additional magnetic measurements (PDF)

Accession Codes

CCDC 2124536–2124540 contain the supplementary crystallographic data for this paper. These data can be obtained free of charge via www.ccdc.cam.ac.uk/data_request/cif, or by emailing data_request@ccdc.cam.ac.uk, or by contacting The Cambridge Crystallographic Data Centre, 12 Union Road, Cambridge CB2 1EZ, UK; fax: +44 1223 336033.

AUTHOR INFORMATION

Corresponding Author

Paul J. Saines — *School of Physical Sciences, University of Kent, Canterbury CT2 7NH, U.K.;* ⓸ orcid.org/0000-0002-4207-2112; Email: P.Saines@kent.ac.uk

Authors

Patrick W. Doheny — *School of Physical Sciences, University of Kent, Canterbury CT2 7NH, U.K.*

Simon J. Cassidy — *Inorganic Chemistry Laboratory, Department of Chemistry, University of Oxford, Oxford OX1 3QR, U.K.;* ⓸ orcid.org/0000-0002-4297-1425

Complete contact information is available at:
https://pubs.acs.org/10.1021/acs.inorgchem.1c03688

Notes

The authors declare no competing financial interest.

REFERENCES

(1) Ladd, T. D.; Jelezko, F.; Laflamme, R.; Nakamura, Y.; Monroe, C.; O'Brien, J. L. Quantum computers. *Nature* **2010**, *464*, 45−53.

(2) Gyongyosi, L.; Imre, S. A Survey on quantum computing technology. *Comput. Sci. Rev.* **2019**, *31*, 51−71.

(3) Cho, A. Helium-3 Shortage Could Put Freeze On Low-Temperature Research. *Science* **2009**, *326*, 778−779.

(4) Smith, A. Who discovered the magnetocaloric effect? *Eur. Phys. J. H* **2013**, *38*, 507−517.

(5) Weiss, P.; Piccard, A. Le phénomène magnétocalorique. *J. Phys. Theor. Appl.* **1917**, *7*, 103−109.

(6) Dixey, R. J. C.; Saines, P. J. Optimization of the Magnetocaloric Effect in Low Applied Magnetic Fields in $LnOHCO_3$ Frameworks. *Inorg. Chem.* **2018**, *57*, 12543−12551.

(7) Wali, M.; Skini, R.; Khlifi, M.; Dhahri, E.; Hlil, E. K. A giant magnetocaloric effect with a tunable temperature transition close to room temperature in Na-deficient La0.8Na0.2−x□xMnO3 manganites. *Dalton Trans.* **2015**, *44*, 12796−12803.

(8) Lyubina, J. Magnetocaloric materials for energy efficient cooling. *J. Phys. D: Appl. Phys.* **2017**, *50*, No. 053002.

(9) Barman, A.; Kar-Narayan, S.; Mukherjee, D. Caloric Effects in Perovskite Oxides. *Adv. Mater. Interfaces* **2019**, *6*, No. 1900291.

(10) Chogondahalli Muniraju, N. K.; Baral, R.; Tian, Y.; Li, R.; Poudel, N.; Gofryk, K.; Barišić, N.; Kiefer, B.; Ross, J. H.; Nair, H. S. Magnetocaloric Effect in a Frustrated Gd-Garnet with No Long-Range Magnetic Order. *Inorg. Chem.* **2020**, *59*, 15144−15153.

(11) Mukherjee, P.; Dutton, S. E. Enhanced Magnetocaloric Effect from Cr Substitution in Ising Lanthanide Gallium Garnets $Ln_3CrGa_4O_{12}$ (Ln = Tb, Dy, Ho). *Adv. Funct. Mater.* **2017**, *27*, No. 1701950.

(12) Lun, H.-J.; Xu, L.; Kong, X.-J.; Long, L.-S.; Zheng, L.-S. A High-Symmetry Double-Shell $Gd_{30}Co_{12}$ Cluster Exhibiting a Large Magnetocaloric Effect. *Inorg. Chem.* **2021**, *60*, 10079−10083.

(13) Li, N.-F.; Lin, Q.-F.; Luo, X.-M.; Cao, J.-P.; Xu, Y. Cl−-Templated Assembly of Novel Peanut-like $Ln_{40}Ni_{44}$ Heterometallic Clusters Exhibiting a Large Magnetocaloric Effect. *Inorg. Chem.* **2019**, *58*, 10883−10889.

(14) Peng, J.-B.; Kong, X.-J.; Zhang, Q.-C.; Orendáč, M.; Prokleška, J.; Ren, Y.-P.; Long, L.-S.; Zheng, Z.; Zheng, L.-S. Beauty, Symmetry,

and Magnetocaloric Effect—Four-Shell Keplerates with 104 Lanthanide Atoms. *J. Am. Chem. Soc.* **2014**, *136*, 17938−17941.

(15) Kurmoo, M. Magnetic metal−organic frameworks. *Chem. Soc. Rev.* **2009**, *38*, 1353−1379.

(16) Espallargas, G. M.; Coronado, E. Magnetic functionalities in MOFs: from the framework to the pore. *Chem. Soc. Rev.* **2018**, *47*, 533−557.

(17) Lorusso, G.; Sharples, J. W.; Palacios, E.; Roubeau, O.; Brechin, E. K.; Sessoli, R.; Rossin, A.; Tuna, F.; McInnes, E. J. L.; Collison, D.; Evangelisti, M. A Dense Metal−Organic Framework for Enhanced Magnetic Refrigeration. *Adv. Mater.* **2013**, *25*, 4653−4656.

(18) Chen, Y.-C.; Qin, L.; Meng, Z.-S.; Yang, D.-F.; Wu, C.; Fu, Z.; Zheng, Y.-Z.; Liu, J.-L.; Tarasenko, R.; Orendáč, M.; Prokleška, J.; Sechovský, V.; Tong, M.-L. Study of a magnetic-cooling material Gd(OH)CO₃. *J. Mater. Chem. A* **2014**, *2*, 9851−9858.

(19) Palacios, E.; Rodríguez-Velamazán, J. A.; Evangelisti, M.; McIntyre, G. J.; Lorusso, G.; Visser, D.; de Jongh, L. J.; Boatner, L. A. Magnetic structure and magnetocalorics of GdPO₄. *Phys. Rev. B* **2014**, *90*, No. 214423.

(20) Kim, T. K.; Lee, K. J.; Choi, M.; Park, N.; Moon, D.; Moon, H. R. Metal−organic frameworks constructed from flexible ditopic ligands: conformational diversity of an aliphatic ligand. *New J. Chem.* **2013**, *37*, 4130−4139.

(21) Trzesowska, A.; Kruszynski, R.; Bartczak, T. J. New bond-valence parameters for lanthanides. *Acta Crystallogr.* **2004**, *60*, 174−178.

(22) Gates-Rector, S.; Blanton, T. The Powder Diffraction File: a quality materials characterization database. *Powder Diffr.* **2019**, *34*, 352−360.

(23) Cliffe, M. J.; Goodwin, A. L. PASCal: a principal axis strain calculator for thermal expansion and compressibility determination. *J. Appl. Crystallogr.* **2012**, *45*, 1321−1329.

(24) Shannon, R. D. Revised effective ionic radii and systematic studies of interatomic distances in halides and chalcogenides. *Acta Crystallogr. A* **1976**, *32*, 751−767.

(25) DeVries, L. D.; Barron, P. M.; Hurley, E. P.; Hu, C.; Choe, W. "Nanoscale Lattice Fence" in a Metal−Organic Framework: Interplay between Hinged Topology and Highly Anisotropic Thermal Response. *J. Am. Chem. Soc.* **2011**, *133*, 14848−14851.

(26) Ogborn, J. M.; Collings, I. E.; Moggach, S. A.; Thompson, A. L.; Goodwin, A. L. Supramolecular mechanics in a metal−organic framework. *Chem. Sci.* **2012**, *3*, 3011−3017.

(27) Collings, I. E.; Tucker, M. G.; Keen, D. A.; Goodwin, A. L. Geometric switching of linear to area negative thermal expansion in uniaxial metal−organic frameworks. *CrystEngComm* **2014**, *16*, 3498−3506.

(28) Collings, I. E.; Hill, J. A.; Cairns, A. B.; Cooper, R. I.; Thompson, A. L.; Parker, J. E.; Tang, C. C.; Goodwin, A. L. Compositional dependence of anomalous thermal expansion in perovskite-like ABX₃ formates. *Dalton Trans.* **2016**, *45*, 4169−4178.

(29) Russell, H. N.; Saunders, F. A. New Regularities in the Spectra of the Alkaline Earths. *Astrophys. J.* **1925**, *61*, 38.

(30) Dixey, R. J. C.; Orlandi, F.; Manuel, P.; Mukherjee, P.; Dutton, S. E.; Saines, P. J. Emergent magnetic order and correlated disorder in formate metal-organic frameworks. *Philos. Trans. R. Soc. A* **2019**, *377*, No. 20190007.

(31) Daudin, B.; Lagnier, R.; Salce, B. Thermodynamic properties of the gadolinium gallium garnet, Gd₃Ga₅O₁₂, between 0.05 and 25 K. *J. Magn. Magn. Mater.* **1982**, *27*, 315−322.

(32) Guo, F.-S.; Leng, J.-D.; Liu, J.-L.; Meng, Z.-S.; Tong, M.-L. Polynuclear and Polymeric Gadolinium Acetate Derivatives with Large Magnetocaloric Effect. *Inorg. Chem.* **2012**, *51*, 405−413.

(33) Lorusso, G.; Palacios, M. A.; Nichol, G. S.; Brechin, E. K.; Roubeau, O.; Evangelisti, M. Increasing the dimensionality of cryogenic molecular coolers: Gd-based polymers and metal−organic frameworks. *Chem. Commun.* **2012**, *48*, 7592−7594.

(34) Saines, P. J.; Paddison, J. A. M.; Thygesen, P. M. M.; Tucker, M. G. Searching beyond Gd for magnetocaloric frameworks: magnetic

properties and interactions of the Ln(HCO₂)₃ series. *Mater. Horiz.* **2015**, *2*, 528−535.

(35) Falsaperna, M.; Stenning, G. B. G.; da Silva, I.; Saines, P. J. Magnetocaloric Ln(HCO₂)(C₂O₄) frameworks: synthesis, structure and magnetic properties. *J. Mater. Chem. C* **2021**, *9*, 13209−13217.

(36) Kelly, N. D.; Liu, C.; Dutton, S. E. Structure and magnetism of a new hexagonal polymorph of Ba₃Tb(BO₃)₃ with a quasi-2D triangular lattice. *J. Solid State Chem.* **2020**, *292*, No. 121640.

(37) Kelly, N. D.; Dutton, S. E. Magnetic Properties of Quasi-One-Dimensional Lanthanide Calcium Oxyborates Ca₄LnO(BO₃)₃. *Inorg. Chem.* **2020**, *59*, 9188−9195.

(38) Mukherjee, P.; Wu, Y.; Lamprontí, G. I.; Dutton, S. E. Magnetic properties of monoclinic lanthanide orthoborates, LnBO₃, Ln = Gd, Tb, Dy, Ho, Er, Yb. *Mater. Res. Bull.* **2018**, *98*, 173−179.

(39) Dixey, R. J. C.; Stenning, G. B. G.; Manuel, P.; Orlandi, F.; Saines, P. J. Ferromagnetic Ising chains in frustrated LnODCO₃: the influence of magnetic structure in magnetocaloric frameworks. *J. Mater. Chem. C* **2019**, *7*, 13111−13119.

(40) *CrysAlisPro*; Rigaku Oxford Diffraction Ltd.: Yarnton, Oxfordshire, England, 2019.

(41) Sheldrick, G. SHELXT - Integrated space-group and crystal-structure determination. *Acta Crystallogr.* **2015**, *71*, 3−8.

(42) Sheldrick, G. Crystal structure refinement with SHELXL. *Acta Crystallogr.* **2015**, *C71*, 3−8.

(43) Dolomanov, O. V.; Bourhis, L. J.; Gildea, R. J.; Howard, J. A. K.; Puschmann, H. OLEX2: a complete structure solution, refinement and analysis program. *J. Appl. Crystallogr.* **2009**, *42*, 339−341.